



Electrostatic Discharge Sensitivity and Resistivity Measurements of Al Nanothermites and Their Fuel and Oxidant Precursors

**David Kelly,* Pascal Beland, Patrick Brousseau,
Catalin Florin Petre**

*Royal Military College of Canada, 11 General Crerar Crescent,
K7K 7B4 Kingston, Canada*

**E-mail: david.kelly@rmc.ca*

Abstract: The sensitivity of nanothermites to electrostatic discharge (ESD) has been noted by many authors. In the present work, nanothermites have been prepared using aluminium fuels with oxide (O-Al), palmitic acid (L-Al) and Viton (V-Al) passivation and CuO, Fe₂O₃ and MoO₃ oxidants, as well as binary oxidant mixtures. Fuel- and oxidant-based ESD sensitivity trends of O-Al ≈ L-Al >> V-Al and MoO₃ >> CuO ≈ Fe₂O₃ were observed with binary oxidants affording intermediate sensitivities. In the majority of cases, with the exception of high proportions of MoO₃ oxidant, nanothermites containing V-Al fuel were the least sensitive to ESD at >0.156 J. Resistivity measurements have been made for the fuels and oxidants and follow the trends V-Al >> O-Al ≈ L-Al and MoO₃ >> Fe₂O₃ > CuO. V-Al resistivity of *ca.* 10¹¹ Ω·cm exceeds that of the oxidants studied. An ESD sensitivity trend, based on a reduced proportion of spark current carried by the aluminium fuel, is proposed and was consistent with the observed ESD and resistivity data.

Keywords: nanothermite, electrostatic discharge sensitivity, resonant acoustic mixing, nano aluminium

1 Introduction

Thermites represent a distinct class of energetic materials in which an elemental fuel and an oxide oxidant exist in a metastable state. On initiation these materials react, moving to a more thermodynamically stable state by the transfer of oxygen. Although thermite reactions often afford large negative enthalpies of reaction [1],

the rates of reaction are significantly slower than those associated with energetic materials; consistent with other systems in which the fuel and oxidant are not present within a single molecule. Whilst the rates of reaction are limited by the diffusion of reactants, the application of nanoscale materials demonstrated the potential of nanothermites in propellant and explosive applications, such as primers [2]. Subsequent research has focused largely on nano aluminium fuel, such material providing large negative enthalpies of reaction with many oxides, realistic production costs and, at least in principal, environmentally benign products [3, 4]. An extensive body of research has investigated the properties and reactivity of nano aluminium, and this work has been recently reviewed [5]. Although aluminium nanothermites have received less attention, a number of workers have performed detailed studies which have delineated the fundamental behaviour of these materials, and these have also been reviewed [5-7].

The potential of nanothermites as energetic materials, particularly as primers, has been established [4, 8]. However, the sensitivity of nanothermites to friction and electrostatic discharge, and to a much lesser extent impact, has also been identified [7]. High sensitivity is an almost inherent characteristic of primer formulations, and components such as lead styphnate display high friction sensitivity [9]. Historical usage has allowed the development of procedures by which lead-based primer formulations may be produced and manipulated. In contrast, the novelty of nanothermites has resulted in the application, production and fundamental studies in parallel. Whilst unintended initiation is rare, such events have occurred and represent a significant impediment to the wider study and use of these materials. Their behaviour with respect to ESD sensitivity, the focus of the present work, and its amelioration are identified in a small number of papers [10-14], but sensitivity is an anticipated feature of nanothermite chemistry. The use of carbon-based materials to reduce ESD sensitivity has been reported [15, 16], whilst recent studies have focused on the relationship between ESD and resistivity in a variety of thermite materials of various particle diameters [17, 18].

Our own interest in nanothermites arises from their potential application as laser initiated primer formulations. To this end, a range of ternary nanothermites based on aluminium fuel and binary oxide mixtures have been produced, as well as binary nanothermites incorporating fuel passivation and/or oxide coatings. More specifically, oxide (O-Al), palmitic acid (L-Al) and Viton (V-Al) coated aluminium were combined, firstly, with CuO, Fe₂O₃ and MoO₃ and, secondly, with binary mixtures of these oxides. The electrostatic discharge sensitivity of these materials has been examined, and in an effect to rationalise these ESD data, the resistivity of the precursor fuel and oxidant precursors have been determined.

2 Methods and Materials

Reagents: All three forms of nano aluminium (O-Al, L-Al and V-Al) were obtained from Reactive Energetics (Montreal, Canada). CuO (< 50 nm), MoO₃ (< 100 nm) and Fe₂O₃ (≈ 50 nm) were obtained from Aldrich (Burlington, Canada). SEM images were used to provide approximate particle dimensions (n = 50). CuO consisted of distorted spheres (44 ± 17 nm) and rods of similar diameter and length 72 ± 12 nm. MoO₃ exhibited a bladed habit (74 ± 36 nm, 173 ± 95 nm and 563 ± 423 nm), whilst Fe₂O₃ was spherical (31 ± 14 nm). Nano aluminium fuels were characterised for their active aluminium content by the NaOH reaction method; other materials were used as received. Total aluminium was measured by instrumental neutron activation analysis at the SLOWPOKE-2 Facility, Royal Military College of Canada.

Nanothermite formation: Mixing was achieved using a lab-scale Resodyn (Butte, USA) Resonant Acoustic Mixer (LabRAM) with 500 g maximum capacity. Conductive ESD containers (LA Packaging, Yorba Linda, USA) were used of diameter 2.5" and height 1" (63.5 × 25.4 mm). These containers were grounded to an external earth. Typical product masses were 0.5–0.7 g, which represents < 1% of the container volume. Mixing conditions were 80 G·min (80 G intensity for 1 min). In general the resultant nanothermites were free-flowing powders, and adhered material was released by gentle agitation. Much higher fractions of container volume are typically employed when mixing high viscosity materials. However, the powders used in the present work do not display significant agglomeration and the principal function of the resonant acoustic mixing is simply to distribute fuel and oxidant through the mixture. Thus, lower fill volumes, with resultant reductions in particle-particle interactions, are attractive for the present application. At this point, the maximum safe container loading densities and minimum mixing times were not established.

Electrostatic discharge measurements. These were made using an in-house system capable of discharges of 5–25 kV and 0.006–0.156 J at 0.50 cm. The system design was similar to described instrumentation [17]. Measurements were made in a vented and electrically insulated box (ca. 50 cm in length, depth and height). Samples were contained within an open cell consisting of a steel base and plastic ring of internal diameter 5.5 mm and depth 1.5 mm. Typical loading densities were 1.2 g·cm⁻³, 1.2 g·cm⁻³ and 2.0 g·cm⁻³ for the CuO, Fe₂O₃, and MoO₃ based nanothermites, respectively. The minimum ignition energy was based on six replicate analyses. Reactions were monitored remotely by video camera.

Resistivity measurements were based on ASTM D 257. Measurements

were made in a Teflon cell with a sample chamber of 6.0 mm length and 3.0 mm² cross section. The measurement cell was attached on a base unit fitted with electrical connections, Figure 1. Although four point measurements are commonly made, a two point system was found acceptable in the present work when tested against a high quality 1 G Ω resistor. The cell and base arrangement facilitated the accurate measurement of sample mass and was found beneficial too for sample cell cleaning. Blank measurements were performed prior to further analyses. A Keysight B2987A electrometer/high resistance meter (Santa Rosa, USA) was used to determine the cell resistance in the mega to teraohm range. Typically at low voltage and high resistance, minimal Joule heating was observed and automated data collection of 10²-10³ measurements was employed to obtain uncertainties below 1%. At higher voltage and lower resistance, data for three independent measurements were obtained with consequent increases in resistance uncertainty. As a maximum current of *ca.* 2 mA can be recorded using the Keysight system, further data were collected using a Slaughter Hipot tester (Lake Forest, USA) and Keithley 6487 picoammeter (Beaverton, USA) at 200 V using the same measurement cell.

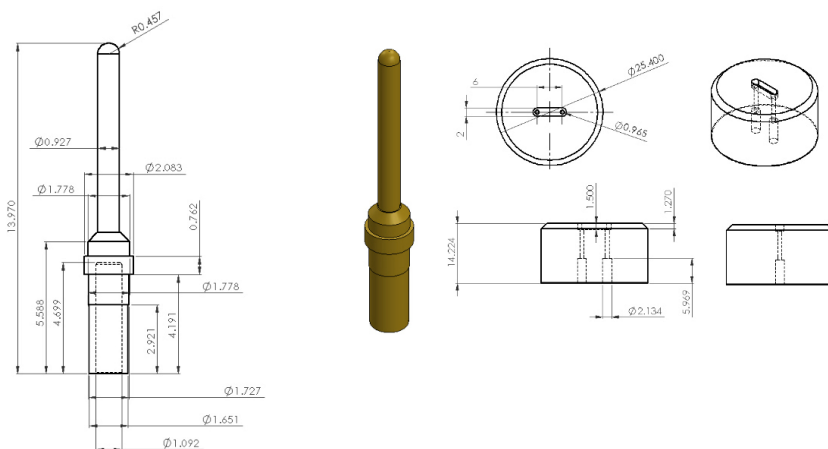


Figure 1. Resistivity test cell schematics

Thermogravimetric data were obtained on a TA Instruments (Castel USA) SDT Q600 instrument, using 2-5 mg samples in alumina crucibles under argon. A heating rate of 10 °C·min⁻¹ was employed over the temperature range 40-1100 °C. A FEI (Hillsboro, USA) Quanta 250 was used to collect SEM images.

3 Results and Discussion

Reagent characteristics. The properties of nano aluminium are critical to performance and those of the nano aluminium common to this work and a series of studies are described elsewhere [19]. In brief, the nano aluminium fuels were of common origin and displayed active aluminium contents of 82.6%, 82.9% and 72.5% for O-Al, L-Al and V-Al, respectively. Total aluminium contents of 90.8%, 92.6% and 82.8% were determined by instrumental neutron activation analysis. Assuming that (i) the mass difference between total and active Al could be assigned to Al₂O₃, and (ii) the volatile mass losses observed by thermogravimetric analysis under argon corresponded to loss of water, hydroxyl dehydration and passivation layer decomposition, total mass balances of 100.0 (0.3)%, 105.3 (3.5)% and 104.0 (4.8)% were obtained for O-Al, L-Al and V-Al, respectively, at one sigma uncertainty. Similar particle sizes and distributions were observed for O-Al, L-Al and V-Al. Thermo-gravimetric analyses provided data suggestive of particle diameters smaller than 100 nm, based on consistent onset melting temperatures of 655 ± 1 °C and enthalpies of fusion of 304-310 J·g⁻¹. SEM images corresponded to a 30-200 nm distribution, with occasional particles greater than 1 μm [19]. SEM images of CuO, Fe₂O₃ and MoO₃ were consistent with their stated particle sizes. Fe₂O₃ was confirmed to be in the gamma form by X-ray diffraction, which also yielded crystallite dimensions of ca. 50 nm.

Nanothermite preparation. Nanothermites are often prepared at non-stoichiometric mole ratios (ϕ) of fuel (F) and oxidant (A), with fuel-rich mixtures often providing optimum performance, Equation 1 [20].

$$\phi = \frac{(F/A)_{actual}}{(F/A)_{stiochiometric}} \quad (1)$$

In the present work $\phi = 1.2$ was used throughout. Where two oxides are employed to provide A , it is also necessary to define the ratio of the oxides used. In Equation 1 the use of ratios means there is no requirement to consider oxidation states. However, the use of fuels of different oxidation state renders this necessary. The actual number of moles of electrons accepted by the oxidant from the fuel is $3F_{actual}/\phi$ or n_F . For a two oxidant system:

$$n_F = n_{A1} \cdot x_1 + n_{A2} \cdot x_2 \quad (2)$$

where n_{A1} and n_{A2} are the moles of oxidant $A1$ and $A2$, and x_1 and x_2 are their respective cation (metal) oxidant states. Thus, the fraction of reacting oxidant, expressed in an oxidation state weighted form, can be defined as;

$$1 = \frac{n_{A1} \cdot x_1}{n_F} + \frac{n_{A2} \cdot x_2}{n_F} = f_1 + f_2 \quad (3)$$

$$\text{where } f_1 = \frac{n_{A1} \cdot x_1}{n_F} \text{ and } f_2 = (1 - f_1) = \frac{n_{A2} \cdot x_2}{n_F}$$

Binary nanothermites were prepared using V-Al, O-Al and L-Al with either MoO₃, CuO or Fe₂O₃, respectively. Ternary nanothermites used metal oxide pairs with $f_1:f_2=0.75:0.25, 0.50:0.50$ and $0.25:0.75$. Further ratios were prepared as necessary. A quantitative assessment of the mixing quality is difficult to obtain. However, the measurement of the reaction enthalpies by TGA/DSC and SEM images provided some information. It is typical that DSC exotherms obtained under argon do not approach the theoretical values [1]. However, for the reaction of O-Al and MoO₃, which is not complicated by potential passivant reactivity, the enthalpy of 2307 kJ·mol⁻¹ [21] is comparable with data obtained from samples mixed using ultrasonic methods in an organic solvent [22] and represents *ca.* 50% of the theoretical value. The reaction of O-Al and CuO affords an enthalpy of 1840 kJ·mol⁻¹ [21], which represents a similar fraction of the theoretical value. It is again comparable with the literature, although the cited work does represent a layered structure [23]. The recorded enthalpy for the O-Al and Fe₂O₃ nanothermite (1739 kJ·mol⁻¹) represents a somewhat smaller fraction of the theoretical value, 37%. SEM images for these three nanothermites, Figure 2, provide further evidence of a high quality of mixing with intimate interactions between fuel and oxidant on nanometre scales. However, it was also observed that, in the absence of a controlling architecture, such nanothermites do not display a fully homogeneous distribution of fuel and oxidant.

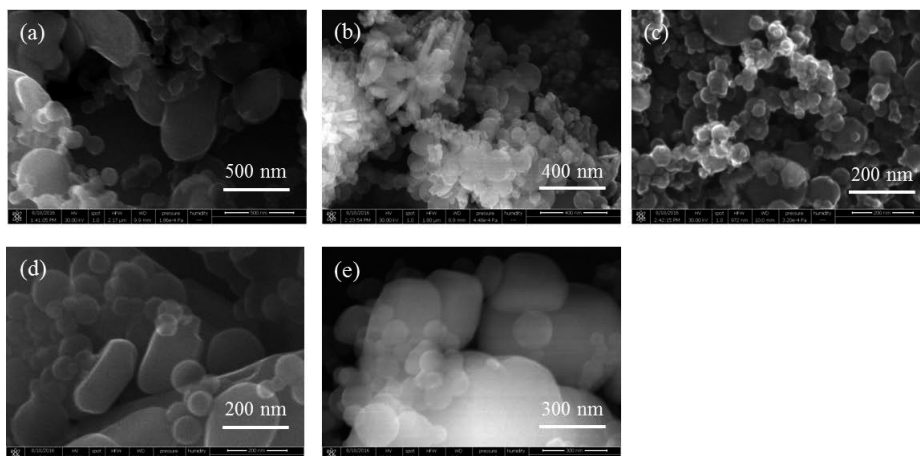


Figure 2. SEM images obtained for nanothermites comprising O-Al and MoO₃ (a), CuO (b) and Fe₂O₃ (c), L-Al and MoO₃ (d), V-Al and MoO₃ (e)

ESD Sensitivity. ESD sensitivity data were obtained for nanothermites based on the three aluminium fuels utilising oxide (O-Al), palmitic acid (L-Al) and Viton (V-Al) passivation in combination with CuO, Fe₂O₃ and MoO₃, and with binary mixtures of these oxides, Table 1. In the field of energetic materials the goal is to produce the least sensitive material and therefore the largest ESD response. The data display a series of trends based on fuel and oxidant as follows:

- (i) a marked decrease in sensitivity of CuO or Fe₂O₃-based systems relative to those of MoO₃. This trend is illustrated by the increase in the minimum ESD response energy down any and all of columns 1-6 in Table 1 as a greater proportion of oxidant is Fe₂O₃ or CuO.
- (ii) a marked decrease in sensitivity for V-Al systems relative to those of O-Al and L-Al, with the latter providing similar data. An example is provided by the comparison of V-Al data (column 2) with those of O-Al and L-Al (columns 1 and 3) for the MoO₃:CuO systems. At any value of $f_1:f_2$, V-Al fuel systems affords lower ESD sensitivity than those of O-Al or L-Al.
- (iii) intermediate sensitivities for mixed oxides relative to their respective single oxide systems for Cu-Mo and Fe-Mo oxides, as illustrated by any one of columns 1-6. However, more complex behaviour for Cu-Fe systems with some examples of enhanced sensitivity for binary oxide mixtures. For example, the O-Al system (column 7) shows greater ESD sensitivity (lower values) for nanothermites containing binary oxides of $f_1:f_2 = 0.75:0.25$, $0.50:0.50$ and $0.25:0.75$, than their single oxide analogues.

The above observations can be placed in the context of published sensitivities. Petre *et al.* [10] observed an oxidant sensitivity trend Bi > Mo >> Cu for L-Al and micrometric oxides, whilst Weir *et al.* [17, 18] observed the reverse trend for Mo and Cu with oxide passivated aluminium fuel. Although the literature data may appear contradictory, it is believed here to simply represent the complex relationship between particle properties and ESD sensitivity. For example, the marked dependence of the physical properties of Fe₂O₃ fuel on the ESD sensitivity of Al/Fe₂O₃ nanothermites have been reported previously [13, 14], with sensitivities of 0.030 and greater than 1.0 J for aerogel and xerogel Fe₂O₃, respectively.

Resistivity measurements. The extent to which nanothermites conduct spark-generated current may be central to the rationalisation of ESD sensitivity. The conductivity of thermite materials has been explored previously [17, 18]. Low voltages were employed (typically 1 V) to avoid resistive heating and nanothermite ignition. To avoid such problems and to have the liberty of using higher voltages, the resistivity of fuel and oxidant has been examined separately in the present work. A voltage range of 0.6 V to 1000 V and packing densities

Table 1. Electrostatic discharge data for Al and CuO, Fe₂O₃ and MoO₃ single and mixed oxide nanothermites

Column	1	2	3	4	5	6	7	8	9		
Oxidant	O-Al	V-Al	L-Al	O-Al	V-Al	L-Al	O-Al	V-Al	L-Al		
MuO ₃	CuO	O-Al	V-Al	L-Al	MuO ₃	Fe ₂ O ₃	O-Al	V-Al	L-Al		
<i>f</i> ₁	<i>f</i> ₂	ESD /J		<i>f</i> ₁	<i>f</i> ₂	ESD /J	<i>f</i> ₁	<i>f</i> ₂	ESD /J		
1.00	0	< 0.006	< 0.006	< 0.006	< 0.006	< 0.006	1.00	0	0.100	> 0.156	> 0.156
0.93	0.07	< 0.006		0.07	0.100		0.93	0.07			
0.87	0.13	< 0.006		0.13	0.100		0.87	0.13			
0.81	0.19	< 0.006		0.19	> 0.156		0.81	0.19			
0.75	0.25	< 0.006	0.025	< 0.006	> 0.156	< 0.006	0.75	0.25	< 0.006	> 0.156	0.156
0.50	0.50	< 0.006	> 0.156	< 0.006	> 0.156	< 0.006	0.50	0.50	0.025	> 0.156	0.025
0.44	0.56	< 0.006		0.56			0.44	0.56	< 0.006		
0.38	0.62	< 0.006		0.62			0.38	0.62	0.056		
0.32	0.68	< 0.006		0.68			0.32	0.68	0.100		
0.25	0.75	0.056	> 0.156	< 0.006	> 0.156	0.056	0.25	0.75	0.056	> 0.156	0.025
0.19	0.81		< 0.006	0.81			0.19	0.81	0.156		
0.13	0.87		< 0.006	0.87			0.13	0.87	> 0.156		
0.07	0.93		< 0.006	0.93			0.07	0.93	> 0.156		
0	1.00	> 0.156	0.025	0	1.00	> 0.156	0	1.00	> 0.156	> 0.156	0.025

spanning those used in the ESD studies were employed (CuO $0.7\text{--}1.7\text{ g}\cdot\text{cm}^{-3}$, Fe_2O_3 $0.5\text{--}1.1\text{ g}\cdot\text{cm}^{-3}$, MoO_3 $1.7\text{--}3.1\text{ g}\cdot\text{cm}^{-3}$, and Al fuels $0.2\text{--}1.2\text{ g}\cdot\text{cm}^{-3}$). The removal of nanothermite ignition risk facilitates the examination of resistivity at a maximum of $1.7\text{ kV}\cdot\text{cm}^{-1}$, which approaches the $4\text{--}30\text{ kV}\cdot\text{cm}^{-1}$ values generally observed in ESD generated sparks [24].

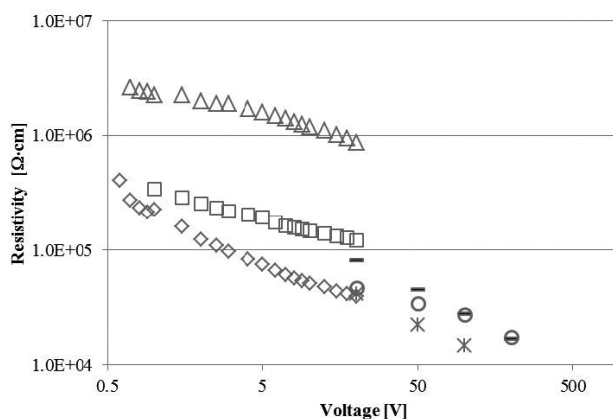


Figure 3. Resistivity data obtain for nano CuO powder as a function of voltage packing density (Δ , $0.806\text{ g}\cdot\text{cm}^{-3}$; \square , $1.02\text{ g}\cdot\text{cm}^{-3}$; \diamond , $1.21\text{ g}\cdot\text{cm}^{-3}$; —, $1.41\text{ g}\cdot\text{cm}^{-3}$; \circ , $1.01\text{ g}\cdot\text{cm}^{-3}$; $*$, $1.61\text{ g}\cdot\text{cm}^{-3}$). Discontinuities at 20 V correspond to the analysis of separate samples with and without high voltage safety interlock.

Resistivity data obtained for CuO is typical of oxidant behaviour, Figure 3. Resistivity is observed to decrease with increasing packing density and with increasing voltage (or voltage gradient). Direct crystal to crystal and near crystal conduction are likely enhanced in each case. CuO resistivities in the range $10^4\text{--}10^7\ \Omega\cdot\text{cm}$ were recorded, which are high when compared with the $10^1\text{--}10^3\ \Omega\cdot\text{cm}$ reported in deposited films [25]. Since packing densities were calculated to be 13–25% of the bulk density, the higher resistivity values appear reasonable. However, reproducibility was found to be poor and often approached one order of magnitude. It is suggested that packing quality also plays an undefined role in resistivity measurements. Thus, the results presented represent typical resistivity performance rather than an intrinsic property of the material. The measured resistivities of Fe_2O_3 and MoO_3 were $10^6\text{--}10^9$ and $10^9\text{--}10^{11}\ \Omega\cdot\text{cm}$, respectively, obtained at 11–18% and, respectively, 41–61% bulk density, with similar dependence on packing and voltage. These values were again higher than the previously reported film, crystal or compressed powder

densities, which were 10^3 - $10^6 \Omega \cdot \text{cm}$ and 10^4 - $10^6 \Omega \cdot \text{cm}$ for Fe_2O_3 and MoO_3 , respectively [26, 27]. The relative resistivities of CuO , Fe_2O_3 and MoO_3 are shown at a potential of 20 V in Figure 4. It is evident that resistivities follow the general trend $\text{CuO} < \text{Fe}_2\text{O}_3 \ll \text{MoO}_3$, although overlay between CuO and Fe_2O_3 data could also be observed.

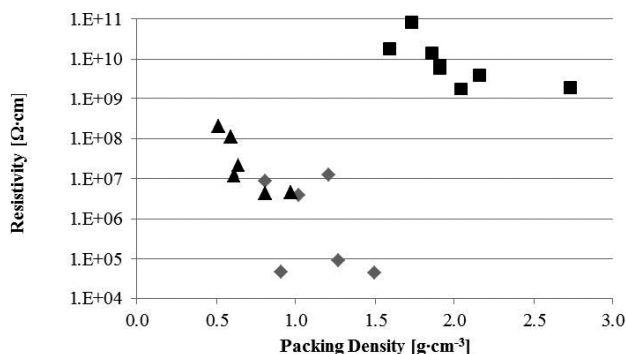


Figure 4. Resistivity measurements for MoO_3 (■), CuO (◆) and Fe_2O_3 (▲) as a function of packing density at 20 V

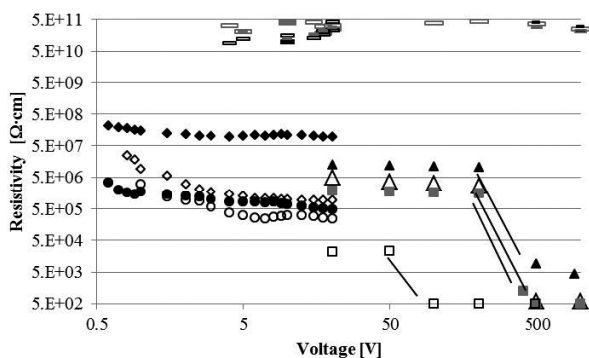


Figure 5. Resistivities of V-Al, shown as cumulative data for varying packing density (solid and open bars), and O-Al (◆, $0.26 \text{ g} \cdot \text{cm}^{-3}$; ◇, $0.40 \text{ g} \cdot \text{cm}^{-3}$; ●, $0.53 \text{ g} \cdot \text{cm}^{-3}$; ○, $0.68 \text{ g} \cdot \text{cm}^{-3}$; ▲, $0.24 \text{ g} \cdot \text{cm}^{-3}$; △, $0.32 \text{ g} \cdot \text{cm}^{-3}$; ■, $0.49 \text{ g} \cdot \text{cm}^{-3}$; □ $0.47 \text{ g} \cdot \text{cm}^{-3}$).

The resistivity of V-Al is distinct from O-Al and L-Al, which in turn showed quite similar behaviour to one another. V-Al displays high resistivity across the entire voltage range studied here. Little or no dependence is observed

as a function of voltage or packing density, so cumulative data for multiple packing densities was combined in Figure 5. Typical resistivities are greater than $10^{11} \Omega \cdot \text{cm}$ and exceed even those of MoO_3 . No literature data is available for V-Al resistivity, although the reduction of nanothermite performance in the presence of Viton has been reported [28]. In contrast, O-Al and L-Al display resistivities in the range 10^5 - $10^8 \Omega \cdot \text{cm}$ that, like the oxidants studied here, show a dependence on both packing density and “quality” and also on applied voltage. Data for O-Al and L-Al were very similar, so only O-Al data was shown in Figure 5. These resistivities reflect the presence of aluminium passivation layers, and are consistent with previously reported data [29]. However, it was found here that at variable applied voltages (typically $> 100 \text{ V}$) resistivities fall below $5 \times 10^2 \Omega \cdot \text{cm}$, a resistivity that reflects the maximum current measured by the Keysight system. Measurements at 200 V using the Slaughter/Keithley system suggested actual resistivities of as low as $10^1 \Omega \cdot \text{cm}$. Thus, a precipitous decrease in resistivity by a factor of 10^4 can occur in these conditions. High resistivity can be re-established over time or by agitation of the sample, suggesting the formation of temporary conductive networks. Conductivity changes cannot easily be related to the bulk heating of the aluminium since, given the nominal conditions in parenthesis ($\rho = 10^6 \Omega \cdot \text{cm}$, $m_{\text{Al}} = 1 \text{ mg}$, $V = 200 \text{ V}$, $\text{time} = 1 \text{ s}$, $C_{\text{pAl}} = 0.900 \text{ J} \cdot \text{K}^{-1} \cdot \text{g}^{-1}$) a bulk heating of less than 5 K will occur. However, local heating cannot be excluded and once lower resistivity is observed ($\rho \approx 10^6 \Omega \cdot \text{cm}$) this heating will be greatly increased. The results suggest the following resistivity order $\text{V-Al} \gg \text{L-Al} \approx \text{O-Al}$, and that L-Al and O-Al can both undergo a *ca.* 10^4 reduction in resistivity at “high” voltage gradients, that are significantly lower than those encountered in ESD discharges. As such, at this reduced resistivity, rapid resistive heating is possible, possibly explaining some of the ESD results reported here, Table 1.

Interpretation of ESD sensitivity and component resistivity

Any interpretation of ESD sensitivity results by analysing the resistivity of constituents must be speculative given that many other factors influence nanothermite reactivity. However, resistivity relates directly to resistive heating and therefore it probably plays a significant role in reaction initiation. The results show that, for any Al fuel used in the present work, ESD sensitivity increases with the increase of the higher resistivity oxidant (*i.e.*, MoO_3), which for binary mixes is coupled with the corresponding decrease of the lower resistivity oxide (*i.e.*, CuO or Fe_2O_3), Table 1. Whilst data are not sufficient to establish a mathematical relationship between oxidant fraction and ESD sensitivity, the observed relationship is incremental and may therefore represent a property of the

sample net oxidant resistivity. Unfortunately, no relationship between ESD and the relatively similar resistivities of CuO and Fe₂O₃ could be determined, since O-Al and L-Al fuels displayed reversed trends, whilst most of V-Al mixtures were found to be insensitive.

As mentioned above, the insensitivity of V-Al systems is almost universal, the exception being the MoO₃-containing systems, which displayed some ESD sensitivity for MoO₃ reacting fractions $f > 0.50$ for CuO and $f > 0.81$ for Fe₂O₃ systems, respectively. In contrast, the majority of O-Al and L-Al systems containing some fraction of MoO₃ display ESD sensitivity below 0.006 J, Table 1. Thus, for these mixes, the ESD sensitivity is reduced by the use of a higher resistivity fuel, a reverse to the observed trend for oxidants.

One rationale for the observation above is based on the supposition that, when exposed to an external spark, nanothermites bear a residual current and voltage, which is different to the one defined by the sample resistance. Thus, the individual resistivities of fuel and oxidant will define the proportion of energy, and therefore resistive heating, applied to them. This model is consistent with the intermediate behaviour of binary oxidant systems. It is also consistent with the high ESD sensitivity of the nanothermite formed by V-Al and MoO₃ in which there is high resistivity for both fuel and oxidant, 10¹¹ Ω·cm and 10⁹-10¹¹ Ω·cm, respectively. This will result in a significant proportion of the current being carried by V-Al. Furthermore, if it is accepted that the resistive heating of the Al fuel coupled with the breakdown of its passivation layer is responsible for the thermite reaction initiation, a high resistivity fuel and low resistivity oxidant will provide the lowest fuel heating and thus the lowest ESD sensitivity. Whilst this hypothesis is consistent with the data presented here, the distinction between correlation and causality must be accepted. However, a factor which supports the hypothesis is that, in the absence of an oxidant, all three nano fuels (V-Al, O-Al and L-Al) are ignited by a spark of 0.156 J and burn in air freely, albeit slowly and incompletely. This observation is consistent with the supposition of greater resistive heating of V-Al in the absence of an oxidant that is able to carry a significant proportion of the applied current.

4 Conclusions

The ESD sensitivity of Al and mixed oxidant nanothermite systems was found to correlate well with the respective resistivity of the oxidant and fuel constituents, with the combination of a high resistivity oxidant and a low resistivity fuel generating the greatest ESD sensitivity. This model is consistent with the

resistive heating of Al fuel as the critical nanothermite initiation step. Moreover, it was found that the use of high resistivity fuel (V-Al) can render the majority of CuO/Fe₂O₃/MoO₃ oxidant combinations insensitive to ESD. The observed variation of resistivity with the packing density and voltage, particularly the marked transition for O-Al and L-Al resistivity, may play a role in the rare but unpredictable ignitions of nanothermites observed by some other workers.

Acknowledgements

Mr. C. McEwen and Mr. B. Ball, Royal Military College of Canada, are thanked for their support in the fabrication and implementation of resistivity measurements. The support of the technical personnel at the Defence Research and Development Canada, Valcartier, in the completion of this work is also gratefully acknowledged.

References

- [1] Fischer, S. H.; Grubelich, M. C. Theoretical Energy Release of Thermites, Intermetallics, and Combustible Metals. *24th International Pyrotechnics Seminar*, Monterey, CA, USA, July 27-31, **1998**.
- [2] Aumann, C. E.; Skofronick, G. L.; Martin, J. A. Oxidation Behavior of Aluminum Nanopowders. *J. Vacuum Sci. Technol. B*, **1995**, *13*: 1178-1183.
- [3] Puszynski, J. A.; Bichay, M. M.; Swiatkiewicz, J. J. *Wet Processing and Loading of Percussion Primers Based on Metastable Nanoenergetic Composites*. Patent US 7,670,446 B2, **2010**.
- [4] Ellis, M. *Environmentally Acceptable Medium Caliber Ammunition Percussion Primers*. US ARDEC Report, SERDP ID WP-1308, **2007**.
- [5] Rossi, C. *Al-based Energetic Materials*. Vol. 2, Wiley, London - New York, **2015**, ISBN: 9781848217171.
- [6] Rossi, C. Two Decades of Research on Nano-Energetic Materials. *Propellants Explos. Pyrotech.* **2014**, *39*: 323-327.
- [7] Piercey, D. G.; Klapötke, T. M. Nanoscale Aluminum – Metal Oxide (Thermite) Reactions for Application in Energetic Materials. *Cent. Eur. J. Energ. Mater.* **2010**, *7*: 115-129.
- [8] Hirlinger, J.; Bichay, M. *Demonstration of Metastable Intermolecular Composites (MIC) on Small Caliber Cartridges and CAD/PAD Percussion Primers*. USARDEC Report ESTCP WP-200205, **2009**.
- [9] Matyáš, R.; Šelešovský, J.; Musil, T. Sensitivity to Friction for Primary Explosives. *J. Hazard. Mater.* **2012**, *213-214*: 236-241.
- [10] Petre, C. F.; Chamberland, D.; Ringuette, T.; Ringuette, S.; Paradis, S.; Stowe, R. Low-Power Laser Ignition of Aluminum/Metal Oxide Nanothermites. *Int. J. Energ.*

- Mat. Chem. Propul.* **2014**, *13*: 479-494.
- [11] Siegert, B.; Comet, M.; Muller, O.; Pourroy, G.; Spitzer, D. Reduced Sensitivity Nanothermites Containing Manganese Oxide Filled Carbon Nanofibers. *J. Phys. Chem. C* **2010**, *114*: 19562-19568.
- [12] Puszynski, J. A.; Bulian, J.; Swiatkiewicz, J. J. Processing and Ignition Characteristics of Aluminium-bismuth Trioxide Nanothermite System. *J. Propul. Power* **2007**, *23*: 698-706.
- [13] Gash, A. E.; Satcher, J. H.; Simpson, R. L.; Clapsaddle, B. J. Nanostructured Energetic Materials with Sol-Gel Methods. *Mat. Res. Soc. Symp. Proc.* **2004**, *800*: AA2.2.1-AA2.2.12.
- [14] Tillotson, T. M.; Gash, A. E.; Simpson, R. L.; Hrubesh, L. W.; Satcher, Jr. J. H.; Poco, J. F. Nanostructured Energetic Materials Using Sol-gel Methodologies. *J. Non-Cryst. Sol.* **2001**, *285*: 338-345.
- [15] Pichot, V.; Comet, M.; Miesch, J.; Spitzer, D. Nanodiamond for Tuning the Properties of Energetic Composites. *J. Hazard. Mater.* **2015**, *300*: 194-201.
- [16] Bach, A.; Gibot, P.; Vidal, L.; Gadiou, R.; Spitzer, D. Modulation of the Reactivity of a WO₃/Al Energetic Material with Graphitized Carbon Black as Additive. *J. Energ. Mater.* **2015**, *33*: 260-276.
- [17] Weir, C.; Pantoya, M. L.; Ramachandran, G.; Dallas, T.; Prentice, D.; Daniels, M. Electrostatic Discharge Sensitivity and Electrical Conductivity of Composite Energetic Materials. *J. Electrostat.* **2013**, *71*: 77-83.
- [18] Weir, C.; Pantoya, M. L.; Daniels, M. The Role of Aluminum Particle Size in Electrostatic Ignition Sensitivity of Composite Energetic Materials. *Combust. Flame* **2013**, *160*: 2279-2281.
- [19] Kelly, D. G.; Beland, P.; Brousseau, P.; Petre, C. F. Formation of Additive-Containing Nanothermites and Modifications to their Friction Sensitivity. *J. Energ. Mater.*, published online doi: 10.1080/07370652.2016.1193072.
- [20] Pantoya, M. L.; Granier, J. J. Combustion Behavior of Highly Energetic Thermites: Nano versus Micron Composites. *Propellants Explos. Pyrotech.* **2005**, *30*: 53-62.
- [21] Kelly, D. G.; Beland, P.; Brousseau, P.; Petre, C. F. The Performance Modification of Aluminum Nanothermites Prepared Using Resonant Acoustic Mixing. *42nd International Pyrotechnics Seminar*, Grand Junction, CO, USA, July 10-15, **2016**.
- [22] Sun, J.; Pantoya, M. L.; Simon, S. L. Dependence of Size and Size Distribution on Reactivity of Aluminum Nanoparticles in Reactions with Oxygen and MoO₃. *Thermochim. Acta* **2006**, *444*: 117-127.
- [23] Petrantoni, M.; Rossi, C.; Conédéra, V.; Bourrier, D.; Alphonse, P.; Tenailleau, C. Synthesis Process of Nanowired Al/CuO Thermite. *J. Phys. Chem. Solids* **2010**, *71*: 80-83.
- [24] Glor, M. Ignition Hazard Due to Static Electricity in Particulate Processes. *Powder Tech.* **2003**, *135-136*: 223-233.
- [25] Meyer, B. K.; Polity, A.; Reppin, D.; Becker, M.; Hering, P.; Klar, P. J.; Sander, Th.; Reindl, C.; Benz, J.; Eickhoff, M.; Heiliger, C.; Heinemann, M.; Bläsing, J.; Krost, A.; Shokovets, S.; Müller, C.; Ronning, C. Binary Copper Oxide

- Semiconductors: From Materials Towards Devices. *Phys. Status Solidi B* **2012**, *249*: 1487-1509.
- [26] Cai, S.; Jian, T. D.; Jin, R.; Zhang, S.; Fujishima, J. A. Semiconductive Properties and Photoelectrochemistry of Iron Oxide Electrodes – VIII. Photoresponses of Sintered Zn-doped Iron Oxide Electrode. *Electrochim. Acta* **1991**, *36*: 1585.
- [27] Hanna, A. A.; Khilla, M. A. Electrical Properties of the Semiconductor Materials Molybdenum and Tungsten Trioxides. *Thermochim. Acta* **1983**, *65*: 311-320.
- [28] Foley, T.; Pacheco, A.; Malchi, J.; Yetter, R.; Higa, K. Development of Nanothermite Composites with Variable Electrostatic Discharge Ignition Thresholds. *Propellants Explos. Pyrotech.* **2007**, *32*: 431-433.
- [29] Lei, X.; Wang, C.; Yi, Z.; Liang, Y.; Sun, J. Effects of Particle Size on the Electrochemical Properties of Aluminum Powders as Anode Materials for Lithium Ion Batteries. *J. Alloy Compds.* **2007**, *429*: 311-315.